Simulation of the Life Cycle of Adsorbate Islands on the Pt(100) Surface during the NO + NH_3 Reaction

Matías Rafti*- José Luis Vicente(1)*
Hannes Uecker†- Ronald Imbihl‡

December 6, 2005

Abstract

Photoemission electron microscopy (PEEM) of the NO + NH_3 reaction on a Pt(100) single crystal surface under UHV conditions reveals complicated dynamical behavior. As a rationalization for the observed spatio-temporal evolution of the surface a so-called "island growth mechanism" was proposed. Here, we present the results of 1D simulations with a realistic 7-variable model. Depending on whether or not we consider site-blocking effects of coadsorbates on diffusing species, we obtain different patterns. The experimental PEEM data can be qualitatively reproduced in this way.

1 Introduction

As a consequence of the deleterious effects on the enviroment the catalytic removal of NO has been the subject of intense research in recent years [2]. Besides this practical aspect catalytic NO reduction also displays interesting dynamical behavior on Pt and Rh surfaces, such as kinetic oscillations and chemical wave patterns [3, 10, 12]. One rather well explored system is the reaction of NO with NH_3 as a reducing agent on a Pt(100) single crystal surface to the main products H_2O and N_2. The results of the studies conducted in an UHV system with Photoemission Electron Microscopy (PEEM), Low Energy Electron Diffraction (LEED), and Work Function measurements [11, 5] can be summarized as follows:

- Sustained temporal oscillations in the reaction rates of N_2 and H_2O formation occur asscociated with corresponding oscillatory variations in surface coverages

*INIFTA, Dto. de Química, Fac. de Cs. Exactas, Universidad Nacional de La Plata, Diag. 113 y 64, CC 16 suc. 4, (1900) La Plata, República Argentina. (1)vicente@inifta.unlp.edu.ar
†Mathematisches Institut I, Universität Karlsruhe, D-76128 Karlsruhe, Germany.
‡Institut für Physikalische Chemie und Elektrochemie, Universität Hannover, Callinstr. 3-3a, D-30167 Hannover, Germany.

- LEED data show that the rate oscillations are associated with a periodic structural change of the surface between a quasi-hexagonal reconstruction ("hex") and the bulk-like 1×1 phase
- PEEM show a variety of chemical wave patterns which include spiral waves and target patterns as well as a cyclic transformation of the surface via two different reaction fronts [11].

The topmost layer of a clean Pt(100) sample reconstructs into a quasi-hexagonal geometry ("hex") but upon adsorption of NO and other gases the reconstruction is lifted and the surface Pt atoms move back into the positions of the bulk-like 1×1 termination. Three different grey levels were identified in PEEM experiments, which were assigned to three different adsorbate phases. An explanation for the cyclic transformation of the surface was proposed by Veser et al. in [11], the so called 'island growth mechanism'.

Two processes were found to be crucial for the occurence of rate oscillations in this system. Firstly, it is the autocatalytic kinetics of NO dissociation as evidenced in the experiments by the appearance of a spike-like rise in reaction rates, the so called 'surface explosion' [4]. The 'explosive' behavior is due to the autocatalytic increase in the number of vacant sites required for NO dissociation to occur. The second key factor is the adsorbate - driven (1×1) $\rightleftharpoons$ hex phase transition between the catalytically inactive hex reconstructed surface and the active bulk-like (1×1)-termination of the surface.

A realistic mathematical model, consisting of seven coupled ordinary differential equations (ODEs), has been proposed by Lombardo et al. to explain the rate oscillations and the hysteresis in the reaction rate that is associated with the (1×1) $\rightleftharpoons$ hex surface phase transition [5]. The ODEs describe the evolution of the local coverages of the six proposed intermediates, namely NO on hex and on (1×1) phase ($\theta_{\mathrm{NO}}^{\mathrm{hex}}$ and $\theta_{\mathrm{NO}}^{1\times1}$), NH_3, N, H, and O on (1×1) phase ($\theta_{\mathrm{NH_3}}^{1\times1}$, $\theta_{\mathrm{N}}^{1\times1}$, $\theta_{\mathrm{H}}^{1\times1}$ and $\theta_{\mathrm{O}}^{1\times1}$), and of the fraction of surface in the 1×1 phase ($\theta_{1\times1}$). The ODE system can be written in abstract form as:

$$\frac{d\mathbf{x}(t)}{dt} = \boldsymbol{f}(\mathbf{x}(t); p, T), \qquad \mathbf{x} \in \mathbb{R}^7, \;\; \boldsymbol{f} = (f_1, f_2, \ldots, f_7), \tag{1}$$

where $\mathbf{x}$(t) is a 7-D vector which represents the coverages, T is the absolute temperature, and $p \in \mathbb{R}^{11}$ is a vector of (fixed) T independent parameters. See [5] or [10, 9, 8] for details. In particular see [10] for a detailed numerical study of these ODE's. Essentially, relaxation oscillations were obtained.

With Fickian diffusion the dynamics of these ODE oscillators was studied numerically in 1D and 2D in [9] and [8], integrating a reaction-diffusion system of the form

$$\frac{\partial \mathbf{x}(t, \mathbf{q})}{\partial t} = \boldsymbol{f}(\mathbf{x}(t, \mathbf{q}); p, T) + \mathbf{M}(T)\nabla^2 \mathbf{x}(t, \mathbf{q}) \tag{2}$$

where $\mathbf{q}$ is the spatial variable and $M(T)$ is a temperature dependent diagonal diffusion matrix. However, although these simulations showed a rich variety of patterns, which were in part similar to the experiment, the overall agreement with the experimental data was rather poor [8].

The following modifications were implemented. First, in order to take into account that the surface concentrations depend on variable sizes of the (1×1) and hex patches, we use local coverages

$$\begin{aligned} X &= (\theta_{1\times1}, \Theta_{\mathrm{NO}}^{hex}, \Theta_{\mathrm{NO}}^{1\times1}, \Theta_{\mathrm{NH_3}}^{1\times1}, \Theta_{\mathrm{O}}^{1\times1}, \Theta_{\mathrm{N}}^{1\times1}, \Theta_{\mathrm{H}}^{1\times1}) \\ &= (\theta_{1\times1}, \theta_{\mathrm{NO}}^{\mathrm{hex}}/\theta_{\mathrm{hex}}, \theta_{\mathrm{NO}}^{1\times1}/\theta_{1\times1}, \theta_{\mathrm{NH_3}}^{1\times1}/\theta_{1\times1}, \theta_{\mathrm{O}}^{1\times1}/\theta_{1\times1}, \theta_{\mathrm{N}}^{1\times1}/\theta_{1\times1}, \theta_{\mathrm{H}}^{1\times1}/\theta_{1\times1}). \end{aligned}$$

Since the diffusional flow is governed by the difference in concentration we use local coverages in the diffusion part of the equations, i.e.

$$\frac{\partial \mathbf{x}(t,\mathbf{q})}{\partial t} = \boldsymbol{f}(\mathbf{x}(t,\mathbf{q}); p, T) + \mathbf{M}(T)\nabla^2\mathbf{X}(t,\mathbf{q}) \tag{3}$$

Secondly, we take into account that diffusion on surfaces is not Fickian because vacant sites are required, i.e. sites not covered by adsorbate. We therefore introduce site blocking [7], which yields a PDE of the form

$$\frac{\partial \mathbf{x}(t,\mathbf{q})}{\partial t} = \boldsymbol{f}(\mathbf{x}(t,\mathbf{q}); p, T) + \mathbf{M}(T)\big[g(\mathbf{X})\cdot\nabla^2\mathbf{X}(t,\mathbf{q}) - \mathbf{X}\cdot\nabla^2 g(\mathbf{X})\big]. \tag{4}$$

Here $g : \mathbb{R}^7 \to \mathbb{R}^7$, where $g_i(X)$ models the effect of coadsorbates on diffusion of the i^{th} species due to site blocking. We show that our model (4), based on the LFI mechanism, can qualitatively reproduce the main features of PEEM experiments in the 1D setting.

The remainder of this work is organized as follows. In section 2 we give a description of the island growth mechanism for the reacting Pt(100) surface, and in section 3 the model used for the simulations is described in more detail. Section 4 is devoted to present our main results. Conclusions are given in section 5.

2 PEEM experiments and island growth mechanism

PEEM experiments have revealed three distinct grey levels associated with different surface adsorbate phases [11].A PEEM image, showing various stages in the island cycle is reproduced in Fig. 1. PEEM images primarily the work function that is oxygen covered areas appear as dark and areas with a reduced work function, i.e. the ammonia covered surface, as bright. The cyclic transformation of the surface we observe in PEEM can be described as follows. On a grey background a dark island nucleates and starts to grow. This dark area only grows to a certain size and then a bright nucleus forms in the interior of the dark island, which then also starts to expand. Thus, two fronts are present, a "dark front", enlarging the island, and a "bright front" eating up the island. The bright front has a higher speed than the dark front, and eventually catches up with the dark front. Behind the bright front the surface gradually returns to its initial grey level.

Based on previous studies of this system a tentative mechanistic description of the PEEM results has been given [11]. The grey levels in PEEM are assigned as follows:

medium grey:	clean hex reconstructed surface
dark area:	(1×1) - NO_{ad}/O_{ad}
bright area:	(1×1) - $NH_{x,ad}$ $(x = 1 - 3)$.

The cyclic transformation of the surface comprises the following steps:

(i) Starting from the clean hex reconstructed surface (medium grey) NO adsorption lifts the hex reconstruction. On the 1×1 thus formed the NO partially dissociates. The dark front accordingly represents the phase transition hex → 1×1 - NO_{ad}/O_{ad}.

(ii) On the (1×1) - NO_{ad}/O_{ad} phase NH_3 can still adsorb and react. Through reactive removal of oxygen finally an $NH_{x,ad}$ $(x = 1-3)$ layer is formed. The second front therefore corresponds to the transition (1×1) - NO_{ad}/O_{ad} → (1×1) - $NH_{x,ad}$ $(x = 1 - 3)$.

(iii) The (1×1)- $NH_{x,ad}$ layer is not stable enough to maintain a 1×1 surface. Continuous reaction and desorption of N_2 generates vacant 1×1 sites which then transform into the hex phase. The gradual surface change bright → medium grey therefore corresponds to the transition (1×1) - $NH_{x,ad}$ → hex.

The hex phase (1×1 phase) is considered to be catalytically inactive (active). Since the different islands grow unsynchronized on the Pt(100) surface the macroscopically measured reaction rate is stationary, despite the fact that an individual life cycle of an island is equivalent to an oscillation cycle.

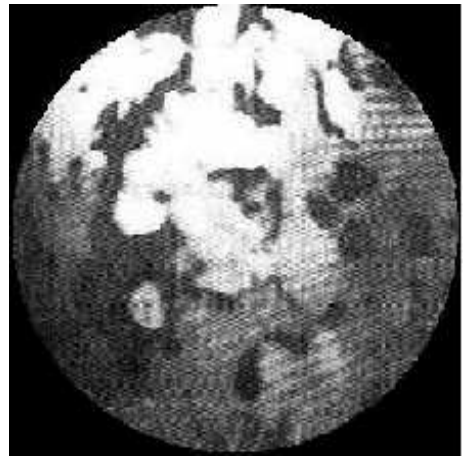

Figure 1: PEEM image showing a cyclic transformation of the Pt(100) surface during the NO + NH_3 reaction. The structural transformations proceed via two types of reaction fronts, grey/black and black/bright with the surface returning continuously from bright back to grey. Grey corresponds to the clean hex reconstructed surface, black to a 1×1 - NO_{ad}/O_{ad}, and bright to a $NH_{x,ad}$ $(x = 1 - 3)$ layer. $T = 438K$, $P_{NO} = 1.3x10^{-6}$ mbar and $P_{NH_3} = 2.1x10^{-6}$ mbar. Image width is 450 μm. [11]

3 Set up for the system

3.1 Diffusion

Diffusion constants of the adsorbates (D_i) were calculated using the Arrhenius law, $D_i = \nu e^{E_i/RT}$, where $\nu = 0.0001 cm^2 s^{-1}$ is a common prefactor, and E_i are the activation energies

Table 1: Estimated activation energies for surface diffusion $\widetilde{E}_i$ and diffusion constants D_i at $T = 420$K, calculated using Arrhenius law. $D_i = \nu \mathrm{e}^{-E_i/RT}$ with a common prefactor $\nu = 10^{-4} cm^2 s^{-1}$.

Adsorbate	Reference	$\widetilde{E}_i$(kJ/mol)	$D_i(\mathrm{cm}^2/\mathrm{s}^{-1})$
NO-1x1	[5]	28	$3.3\mathrm{x}10^{-7}$
NO-hex	[5]	22	$1.8\mathrm{x}10^{-6}$
NH_3–1x1	[5]	15	$1.4\mathrm{x}10^{-5}$
N-1x1	[1]	87	$1.5\mathrm{x}10^{-14}$
O-1x1	[1]	150	$2.2\mathrm{x}10^{-22}$
H-1x1	[1]	18	$5.8\mathrm{x}10^{-6}$

for surface diffusion of each species. Due to the lack of experimental data for the diffusion energies of adsorbates on a Pt(100) surface, we make the following assumptions. For the activation barriers of diffusing NO (on both, hex and 1×1 phase) and NH_3 we estimate 25% of their adsorption energies [12]. For N, H and O we use experimental values obtained in chemically similar systems [1].

Table 1 shows the values for the activation energies for the surface diffusion and the calculated diffusion constants. According to these values, we can consider N and O as being immobile, since their diffusion constant values are several orders of magnitude smaller than those of the rest of the adsorbates. Also, since the hex $\leftrightarrow$ 1×1 phase transition is not diffusive, $D_{1\mathrm{x}1} = 0$.

3.2 Site blocking effects

A realistic feature that we add to the model is the so-called "site-blocking effect", succesfully applied before in chemically similar systems (see Evans et al. [7] and references therein). The traditional approach to surface diffusion through Fick's second law ignores the influence of coadsorbed species. Then one obtains (3) simply by adding $M(T)\nabla^2 X$ into (1). This is a rather idealized situation since the diffusivity of each adsorbate should depend at least on the coverages of all coadsorbed species. In order to take this into account we proceed as follows. First, we distinguish between sites for molecular and for atomic adsorbates, and then we include into (3) the non-Fickian terms due to site-blocking:

$$\frac{\partial \theta_i}{\partial t} = f_i + \mathrm{D}_i(\Theta_{\mathrm{diff,i}}\nabla^2\Theta_{\mathrm{i}} - \Theta_{\mathrm{i}}\nabla^2\Theta_{\mathrm{diff,i}}). \tag{5}$$

Here we use the usual nomenclature for coverages: $\Theta_{\mathrm{diff},i}$ is the concentration of vacant sites available for diffusion of the mobile adsorbate i, namely

$$\begin{aligned}
\Theta_{\mathrm{diff},NO} &= \max\{1 - \beta_{NO}^{NO}\Theta_{\mathrm{NO}}^{1\times1} - \beta_{NO}^{NH_3}\Theta_{NH_3}^{1x1}, 0\},\\
\Theta_{\mathrm{diff},NH_3} &= \max\{1 - \beta_{NH_3}^{NO}\Theta_{NO}^{1x1} - \beta_{NH_3}^{NH_3}\Theta_{NH_3}^{1x1}, 0\},\\
\Theta_{\mathrm{diff,H}} &= \max\{1 - \alpha_H^O\Theta_O^{1x1} - \alpha_H^N\Theta_N^{1x1} - \alpha_H^H\Theta_H^{1x1}, 0\}.
\end{aligned} \tag{6}$$

The seven parameters β_i^j and α_i^j control site-blocking effects of the coadsorbed species on the rate of diffusion, and naturally (5) reduces to (3) when $\beta_i^j = \alpha_i^j = 0$. In (6), concentration of vacant sites is assumed to depend linearly on adsorbate coverages. Moreover, $\Theta_{\text{diff},H}$ only includes blocking effects of atomic adsorbates, because we consider atomic and molecular sites on the substrate separately. For the sake of brevity, we will refer to these parameters in the following way:

$$\begin{pmatrix} \beta_{NO}^{NO} & \beta_{NO}^{NH_3} & - \\ \beta_{NH_3}^{NO} & \beta_{NH_3}^{NH_3} & - \\ \alpha_H^O & \alpha_H^N & \alpha_H^H \end{pmatrix}. \tag{7}$$

As in [10, 9, 8] we fix partial pressures of NO and NH_3 to 1.1x10^{-6} and 4.7x10^{-6} mbar respectively, and temperature to 420 K.

To integrate (5) we choose a system of size L in cm and consider n oscillators of size L/n. We choose periodic boundary conditions, discretize in space with finite differences and use the NAG routine D02NDF for time integration.

4 Simulations

4.1 Introduction of surface defects

Chemical waves in surface reactions typically nucleate at macroscopic surface defects. It can be assumed that such a defect region cannot reconstruct but remains in the catalytically active 1×1 state. We model this situation by using two different approaches concerning the introduction of the defect region into the system.

First, we add localized and momentary perturbations to a stable periodic orbit [9]. This is, we first assign a low $\theta_{1\times1}$ coverage value to all oscillators in the domain, and then introduce a perturbation (i.e. a temporal jump in the $\theta_{1\times1}$ value) in the center region of the domain. Results obtained this way are shown in sec. 4.2. Experimentally, such a temporary perturbation may be realized by heating with a laser beam.

An evident shortcoming of the above approach is that on catalytic surfaces defects are typically permanent. In order to model these permanent surface defects we use different values for constants to characterize catalyic properties inside and outside a defect region. Simulations using this second approach are presented in sec. 4.4.

4.2 Temporal perturbations: transition between two regimes

We first analyze the behaviour of (4) using localized perturbations of a stable periodic orbit with low $\theta_{1\times1}$ coverage as initial conditions. Using the traditional reaction-diffusion approach (2) to the reaction system (1), and applying a perturbation of the order of magnitude expected in a hex $\leftrightarrow$ 1×1 phase transition (0.2-0.3 ML [10]), clustering of the surface is obtained [9]. This is, the surface organizes into macroscopic areas (clusters) of roughly the same size in such a way that the phase is constant in each cluster and jumps by half a period from one cluster to the next occur. No frontlike transition is

observed whatsoever. The same happens for the model (3) which corresponds to (4) with the additional blocking parameters

$$\begin{pmatrix} 0 & 0 & - \\ 0 & 0 & - \\ 0 & 0 & 0 \end{pmatrix}, \tag{8}$$

see Fig. 2. Here and in the following, results are presented in grey scale plots, where horizontal and vertical axis are time (t) and space (x), respectively. Greyscales are linear interpolations between z_{min} = black and z_{max} = white, where z stands for the coverage of a given surface intermediate, θ_i (in this case the fraction of the surface in the 1×1 phase ($\theta_{1\times1}$)).

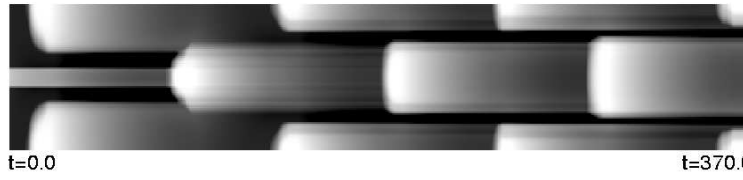

Figure 2: 1-D simulation showing clustering in the oscillatory parameter range of the reaction with simple Fickian diffusion. Equation (4) was integrated (4) with n=80 oscillators and dx=0.00025cm, hence L=0.02cm. Here z stands for $\theta_{1\times1}$, with $z_{max} = 0.70$ and $z_{min} = 0.20$ ML corresponding to white and black respectively. Diffusion constants as shown in Table 1, initial conditions according to sec.4.2 and site blocking constants all set to zero. Periodic boundary conditions (PBC) were applied.

The experimental data in [11] reported spatial structures of a typical size of 0.001 - 0.005 cm; regarding this we use in our simulations $n = 80$ ODE oscillators of size $dx = 0.00025$ cm, total spatial length is therefore $L = 0.02$ cm. Convergence in dx was checked by reducing dx by a factor of two. The number of oscillators is set to $n = 80$ to obtain a system size which allows us to compare simulation with experimental data. Also, using $n = 80$ gives fast results and short transient behaviour.

We estimate the values for the site-blocking parameters of our system as

$$\begin{pmatrix} 1.0 & 1.7 & - \\ 1.5 & 1.0 & - \\ 2.0 & 2.0 & 1.0 \end{pmatrix}. \tag{9}$$

The diagonal elements (β_{NO}^{NO}, $\beta_{NH_3}^{NH_3}$ and α_H^H) are set equal to unity since they stand for site-blocking of an adsorbate by itself. We suppose that N_{ads} and O_{ads} have the same blocking effect on diffusing H_{ads}, and we set $\alpha_H^O = \alpha_H^N = 2.0$ using as guideline the values used in [6]. In a chemically similar reaction system, Rh(110)/NO+H_2, these values were used for O_{ads} site-blocking effect on diffusing H_{ads}. Finally, the values $\beta_{NO}^{NH_3} = 1.7$ and $\beta_{NH_3}^{NO} = 1.5$, were obtained by fitting the simulation results to experimental data. As we will discuss later, we found a much stronger dependence of the system behavior on the value of $\beta_{NO}^{NH_3}$ than on the parameter $\beta_{NH_3}^{NO}$. Further increase of $\beta_{NO}^{NH_3}$ (and hence of

the site-blocking effect of NH_{3ads} on NO_{ads}) yields no significant changes in the results. Using (9) as parameters sharp front-like transitions are observed propagating outwards from the perturbed area as displayed in Fig. 3(a). These fronts, however, vanish almost completely within two or three periods in surface oscillation and the surface returns to a homogeneously oscillating state. A full characterization of the dynamic behaviour of the system for different site-blocking parameters is practically impossible. Since the system is extremely sensitive to changes in $\theta_{\mathrm{NO}}^{1\times1}$ we performed a slow variation of the site blocking of NO diffusion by coadsorbed NH_3 represented by ($\beta_{NO}^{NH_3}$). We obtained patterns which lie in between the two extrema, clustering and front like transitions depicted in Figures 2 and 3(a). Results can be seen in Fig. 3(b)–(d).

(a) parameters from (9)

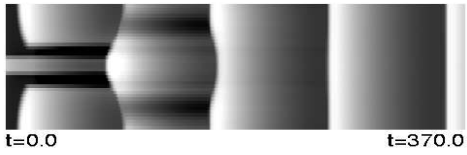

(b) $\beta_{NO}^{NH_3} = 1.55$

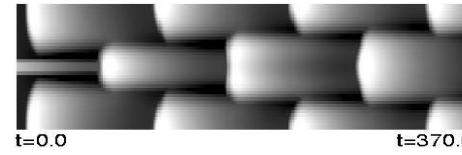

(c) $\beta_{NO}^{NH_3} = 1.58$

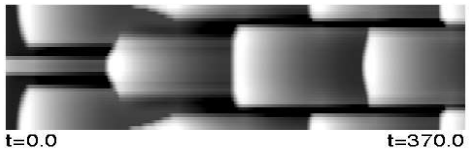

(d) $\beta_{NO}^{NH_3} = 1.61$

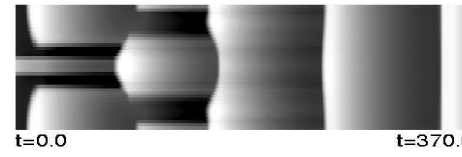

Figure 3: 1-D simulation with non-Fickian diffusion showing the development of reaction fronts as transient phenomena under oscillatory conditions. $\theta_{1\times1}$ is plotted in the graphs. A temporary perturbation of θ_{1x1} in the center was used to mimic the effect of surface defects. (a) same parameters as in Figure 2, except for site blocking constants set to (9). (b)–(d) demonstrate the influence of the parameter $\beta_{NO}^{NH_3}$ on the character of the solution. For $\beta_{NO}^{NH_3} < 1.55$ and $\beta_{NO}^{NH_3} > 1.61$, respectively, clustering and front-like response of the surface time evolution with the same initial conditions is observed.

4.3 ODE orbits

In order to understand the surface clustering behind the front-line transitions we plot in Fig. 4 the time evolution of the coverages (roughly one period) from the ODE's.

The time evolution in Fig. 4 is practically identical with the time evolution at any fixed spatial point in the $x - t$ plots. Starting with a clean hex surface, a growing NO coverage indicates the phase transition from the hex to the 1×1 phase. On the 1×1 phase NO can dissociate into atomic oxygen and nitrogen. Therefore, the relatively sharp transition hex $\rightarrow$ 1×1 is associated with a correspondingly steep increase in the oxygen coverage. Translated into the spatial dimensions this is equivalent to an island growth of the $1\times1/NO_{ad}/O_{ad}$ phase with the steep gradient corresponding to the front grey to black in PEEM (see Fig. [11]). The coverages in Fig. 4 exhibit a second sharp transition when

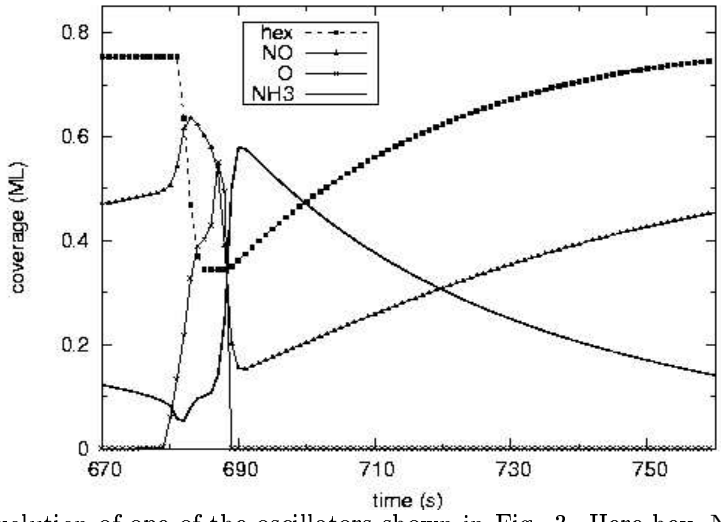

Figure 4: Time evolution of one of the oscillators shown in Fig. 3. Here hex, NO, O, and NH_3 stand for $\theta_{\rm hex}$, $\theta_{\rm NO}^{1\times1}$, $\theta_{\rm O}^{1\times1}$, and $\theta_{\rm NH_3}^{1\times1}$. ML scale in vertical axis corresponds to $\theta_{\rm hex}$ while the rest of the species coverages showed were multiplied here by arbitrary scale factors namely, $\gamma_{NO} = 1.5$, $\gamma_O = 30$ and $\gamma_{NH3} = 5$.

ammonia starts to adsorb and react on the NO/O covered 1×1 phase, causing a steep decrease in the NO/O coverage which is associated with a correspondingly sharp rise of the ammonia coverage. This transition, as will be shown in more detail below, corresponds to the second front, causing a change from dark to bright in PEEM (see Fig. [11]). The reaction between adsorbed species which generates N_2 and H_2O causes a decreasing adsorbate coverage. With the 1×1 phase being no longer stabilized by adsorbate the surface reconstructs back into the hex phase until the initial situation is reached again. Note that this transition proceeds continously and this is what we also see in PEEM: a continuous transition from bright to grey (see Fig. [11]).

4.4 Permanent perturbations: 1D simulations vs PEEM experiments

As explained in sec. 4.1, introducing a permanent defect mimics the situation in the PEEM images where islands and waves typically nucleate at permanent surface defects (see Fig. 1). In Fig. 5 we illustrate the results obtained when a permanent defect region in the center of the cluster is set. We fix the parameters values in order to get an oscillating regime inside the defect region and a non-oscillating regime outside. In detail, outside the center we increase $\theta_{\rm def}$ from the original value of 0.0001 to 0.01 ML and decrease the activation energy E_2 for NO dissociation from 28.5 to 25 kcal/mol^{-1}; see [10] for the effects of these parameters in the ODEs (1). The initial conditions are the same for the whole domain. After some initial transient period the central region emits propagating reaction fronts that propagate outwards to the boundaries of the domain. Moreover, different from the spatially homogeneous phase transitions obtained using a temporal perturbation in sec. 4.2, the system now relaxes into a state in which fronts are emitted periodically.

(a) $\theta_{1\times1}$ (b) $\theta^{1\times1}_{NH_3}$

Figure 5: 1-D simulation with non-Fickian diffusion showing the development of reaction fronts as stable response. A permanent perturbation via modification of the PDE parameters in the center was used to mimic the effect of surface defects. Initial conditions (ic's) are set homogeneously. Same parameters as in Figure 2 were used. Site blocking constants set to (9). PBC applied. (top) $\theta_{1\times1}$, with $z_{max} = 0.70$ and $z_{min} = 0.20$ ML, (bottom) $\theta^{1\times1}_{NH_3}$, with $z_{max} = 0.20$ and $z_{min} = 0.02$ ML. Note the higher velocity of this second front in agreement with PEEM experiments.

The two types of fronts are also illustrated in Fig.6, which displays enlarged sections of Fig. 5(a). The slowing down of the fronts towards the domain boundaries is the result of the PBC's applied i.e. of the collision of the two fronts at the domain boundaries. The plot of $\theta_{1\times1}$ in Fig. 6(a) shows the propagation of the primary front which in the PEEM images corresponds to a front grey/black. The secondary front is not visible in the $\theta_{1\times1}$ plot because it is only connected with a sharp change in the adsorbate coverages but not in the substrate structure. However, it can be visualized in a plot of $\theta^{1\times1}_{NH_3}$ displayed in Fig. 6(b). As in the PEEM images this front appears as transition black/bright. The third transition in the cyclic transformation of the surface structure is the transition $1\times1 \rightarrow$ hex and this transition proceeds spatially uniform, both in the simulations and the experiment. A plot of the spatial concentration profiles is rather similar to Fig. 4 and therefore not reproduced here.

One very striking difference between primary and secondary front is the much higher front velocity of the latter which is faster by roughly a factor of two. This difference is reproduced in the simulations yielding front velocities of 6 μm/s and 15 μm/s for the primary and secondary front, respectively. The ratio of the experimental front velocities are thus reproduced as demonstrated by Table 2, summarizing observed and calculated front velocities. The quantitative difference between experimental and simulated front velocities has its origin in the lack of precise and reliable data for the diffusion constants. The uncertainty therein which is estimated to amount to several orders of magnitude can easily explain the quantitative differences.

5 Summary and Outlook

Our new realistic model of the NO + NH_3 reaction on Pt(100) can reproduce the essential qualititative features of the experiment. The mechanistic interpretation of the different fronts and transitions we observe in PEEM - primary and secondary front plus a spatially uniform phase transition - has thus been put on a solid basis.

We found that adding site-blocking effects for the diffusion species to the model is

(a) $\theta_{1\times1}, z_{scale} = 0.2, 0.7$ (b) $\theta^{1\times1}_{NH_3}, z_{scale} = 0.02, 0.2$

Figure 6: Primary and secondary reaction fronts visualized by plots of $\theta_{1\times1}$ (a) and $\theta^{1\times1}_{NH_3}$ (b). The two plots show an enlarged section of Fig. 5. The differetn front velocities show up by different angles of the white cones.

Table 2: Comparison between velocities of propagation of the first and second front in the experiments and in simulations. For calculation of the front velocities only the constant speed inner zone is considered. Experimental data from ref [11].

	First Front (μm/s)	Second Front (μm/s)
Experiments	0.5	1.10
Simulations	6.0	15.0

essential. With simple Fickian diffusion only clustering but no front-like solutions are obtained. Since almost no experimental data for adsorbate diffusion and in particular, no data for the effect of coadsorbed species on diffusion are available, we had to estimate the site-blocking parameters based on simple physical arguments and chemical intuition. This is clearly a weak point of our simulation and future progress will probably depend on how well this gap can be filled, either by quantum chemical simulations or by new experiments. In agreement with previous simulations we found the reaction system to be extremely sensitive to changes in the parameters describing diffusion of $\theta^{1\times1}_{NO}$. Further work will be oriented towards constructing a two-dimensional model using the characterization of site-blocking parameter space for this reaction system.

Acknowlegments: MR and JLV acknowledges financial support of UNLP (Universidad Nacional de La Plata), CICPBA (Comisión de Investigaciones Científicas de la Prov. de Buenos Aires), and CONICET (Consejo de Investigaciones Científicas y Tecnológicas).

References

[1] J B Barth. Transport of adsorbates at metal surfaces: from thermal migration to hot precursors. *Surf. Sci. Rep.*, 40:75–149, 2000.

[2] W F Egelhoff(Jr.). Fundamental studies of heterogeneous catalysis. In D A King and D P Woodruf, editors, *The Chemical Physics of Solid Surfaces and Heterogeneous*

Catalysis, volume 4. Elsevier, Amsterdam, 1982.

[3] R Imbihl and G Ertl. Oscillatory kinetics in heterogeneous catalysis. *Chem. Rev.*, 95:697–733, 1995.

[4] S J Lombardo, F Esch, and R Imbihl. The NO+NH_3 reaction on Pt(100): steady state and oscillatory kinetics. *Surf. Sci. Lett.*, 271(3):L367–L372, 1992.

[5] S J Lombardo, T Fink, and R Imbihl. Simulations of the NO+NH_3 and NO+H_2 on Pt(100): Steady state and oscillatory kinetics. *J. Chem. Phys.*, 98(7):5526, 1993.

[6] A Makeev and R Imbihl. Simulations of anisotropic front propagation in the O_2+H_2 reaction on a Rh(110) surface. *J. Chem. Phys.*, 113(9):3854–3863, 2000.

[7] M. Tammaro and J.W. Evans. Reactive removal of unstable mixed NO+CO adlayers: Chemical diffusion and reaction front propagation. *J. Chem. Phys.*, 108(18):7795–7806, 1998.

[8] H Uecker. Pattern formation for NO+NH_3 on Pt(100) - two-dimensional numerical results. *Phys. Rev. E*, 71:016207–1,016207–14, 2004.

[9] H Uecker. Standing waves, clustering, and phase waves in 1d simulations of kinetic relaxation oscillations in NO+NH_3 on Pt(100) coupled by diffusion. *Phys. D*, 190:249–265, 2004.

[10] H Uecker, R Imbihl, M Rafti, I M Irurzun, J L Vicente, and E E Mola. Adiabatic reduction and hysteresis of the LFI model for NO + NH_3 on Pt(100). *Chem. Phys. Lett.*, 382:232–244, 2003.

[11] G Vesser, F Esch, and R Imbihl. Regular and irregular spatial patterns in the catalytic reduction of NO with NH_3 on Pt(100). *Cat. Lett.*, 13:371–382, 1992.

[12] V P Zhdanov. Impact of surface science on the understanding of kinectics of heterogeneous catalytic reactions. *Surface Science*, 500:966–985, 2002.